Liquid behavior of cross-linked actin bundles

Kimberly L. Weirich[a], Shiladitya Banerjee[a,b,c], Kinjal Dasbiswas[a], Thomas A. Witten[a,d], Suriyanarayanan Vaikuntanathan[a,e], and Margaret L. Gardel[a,d,f,1]

[a]James Franck Institute, University of Chicago, Chicago, IL 60637; [b]Department of Physics and Astronomy, University College London, London WC1E 6BT, United Kingdom; [c]Institute for the Physics of Living Systems, University College London, London WC1E 6BT, United Kingdom; [d]Department of Physics, University of Chicago, Chicago, IL 60637; [e]Department of Chemistry, University of Chicago, Chicago, IL 60637; and [f]Institute for Biophysical Dynamics, University of Chicago, Chicago, IL 60637

Edited by David A. Weitz, Harvard University, Cambridge, MA, and approved January 10, 2017 (received for review September 28, 2016)

The actin cytoskeleton is a critical regulator of cytoplasmic architecture and mechanics, essential in a myriad of physiological processes. Here we demonstrate a liquid phase of actin filaments in the presence of the physiological cross-linker, filamin. Filamin condenses short actin filaments into spindle-shaped droplets, or tactoids, with shape dynamics consistent with a continuum model of anisotropic liquids. We find that cross-linker density controls the droplet shape and deformation timescales, consistent with a variable interfacial tension and viscosity. Near the liquid–solid transition, cross-linked actin bundles show behaviors reminiscent of fluid threads, including capillary instabilities and contraction. These data reveal a liquid droplet phase of actin, demixed from the surrounding solution and dominated by interfacial tension. These results suggest a mechanism to control organization, morphology, and dynamics of the actin cytoskeleton.

actin | phase separation | liquid crystal | cytoskeleton

The cellular cytoplasm is a hierarchical array of diverse, soft materials assembled from biological molecules that work in concert to support cell physiology (1). The actin cytoskeleton constitutes a spectrum of materials constructed from the semiflexible polymer actin (F-actin) that are crucial in diverse physical processes ranging from cell division and migration to tissue morphogenesis (2, 3). Cross-linking and regulatory proteins assemble actin filaments into bundles and networks with varied composition, mechanics, and physiological function (4). The mechanical properties of actin assemblies regulate force generation and transmission to dynamically control morphogenic processes from the subcellular to tissue length scales (5, 6).

A mechanistic understanding of cytoplasmic mechanics is obscured by the rich complexity of in vivo cytoskeletal assemblies (7) and has been investigated via in vitro model systems (8, 9). Vastly different material properties have been accessed through varying filament length, concentration, and cross-linking. For semidilute concentrations of long actin filaments (>1 μm), the mean spacing between actin filaments, or mesh size, is much smaller than the filament length. In this case, cross-linking proteins mechanically constrain actin filaments to result in space-spanning networks that are viscoelastic gels (10). The structure of cross-linked actin networks is kinetically determined, reflecting a metastable state (11, 12) that requires motor-driven stresses for significant shape changes (13). In contrast, highly concentrated solutions of short actin filaments (<1 μm) align due to entropic effects and form equilibrium liquid crystal phases (14). Liquid crystal theory has been introduced as a framework to understand actin cortex mechanics and mitotic spindle shape (5, 15), but the existence of liquid crystal-like phases at physiological conditions is uncertain.

Liquid-like phases of proteins and nucleic acids have been found within the cytoplasm and are thought to be important in subcellular organization (16). Weak and transient interactions trigger these biomolecules to phase separate from the cytoplasm into droplets, with shape and dynamics dominated by interfacial tension and viscosity (16). Here we demonstrate liquid droplets comprised of cross-linked, short actin filaments. We focus on dilute actin concentrations where cross-linkers are critical to induce phase separation of actin into droplets with tunable tactoid shape. Consistent with a liquid composed of rods, we can describe the droplet shape and dynamics with an anisotropic liquid continuum model. Finally, we demonstrate actin bundles that exhibit shape changes reminiscent of fluid threads, with interfacial tension driven pearling and shortening. This reveals a liquid droplet phase of actin, demixed from the surrounding solution, with shape dominated by interfacial tension.

Results

Liquid Droplets Formed by Short Actin Filaments Cross-Linked by Filamin. We polymerize actin filaments beginning with a dilute (2.6 μM) suspension of actin monomers in the presence of capping protein, which limits filament growth (17). Under these conditions, the average distance between filaments, or mesh size, is ∼1 μm (18) and much larger than the average F-actin length, ∼180 nm, such that filaments freely diffuse and form a uniform, isotropic mixture (Fig. 1*A*, *Left*; *SI Text*; and Movie S1). Adding 0.26 μM of the F-actin cross-linker filamin (19) triggers sudden density changes in the mixture. Actin filaments rapidly assemble into spindle-shaped aggregates of high density, estimated to be 250-μM monomeric actin; a negligible density of filaments remain in the bulk (Fig. 1*B*, *Left*). The tactoids grow over time, increasing in length from ∼1 to 4 μm during the first 60 min after filamin addition (Fig. 1*A* and Movie S1).

These aggregates have a characteristic spindle shape, mathematically described as a tactoid, which is a signature shape of liquid crystal droplets (20). Liquid crystal phases form in highly

Significance

The interior of biological cells is composed of soft, macromolecular-based materials. The semiflexible biopolymer actin cross-links into networks and bundles with diverse architectures to form the actin cytoskeleton. Actin networks have been traditionally thought to be viscoelastic gels, whose rigidity controls cell morphogenesis. Here we demonstrate that cross-linked actin filaments also form liquid droplets. Because these liquids are composed of rod-like polymers, they form anisotropic liquid droplets with a spindle-like shape, whose morphology can be controlled by cross-link concentration. Actin-based liquid bundles also display shape instabilities characteristic of fluids. These shape dynamics reveal a mechanism to control subcellular compartmentalization and dynamics, with implications for mitotic spindle shape and molecular motor-independent contractility.

Author contributions: K.L.W., S.B., S.V., and M.L.G. designed research; K.L.W. performed experiments; S.B. and K.D. developed the model; K.L.W., S.B., K.D., T.A.W., S.V., and M.L.G. contributed new reagents/analytic tools; K.L.W., S.B., and K.D. analyzed data; and K.L.W., S.B., K.D., S.V., and M.L.G. wrote the paper.

The authors declare no conflict of interest.

This article is a PNAS Direct Submission.

[1]To whom correspondence should be addressed. Email: gardel@uchicago.edu.

This article contains supporting information online at www.pnas.org/lookup/suppl/doi:10.1073/pnas.1616133114/-/DCSupplemental.

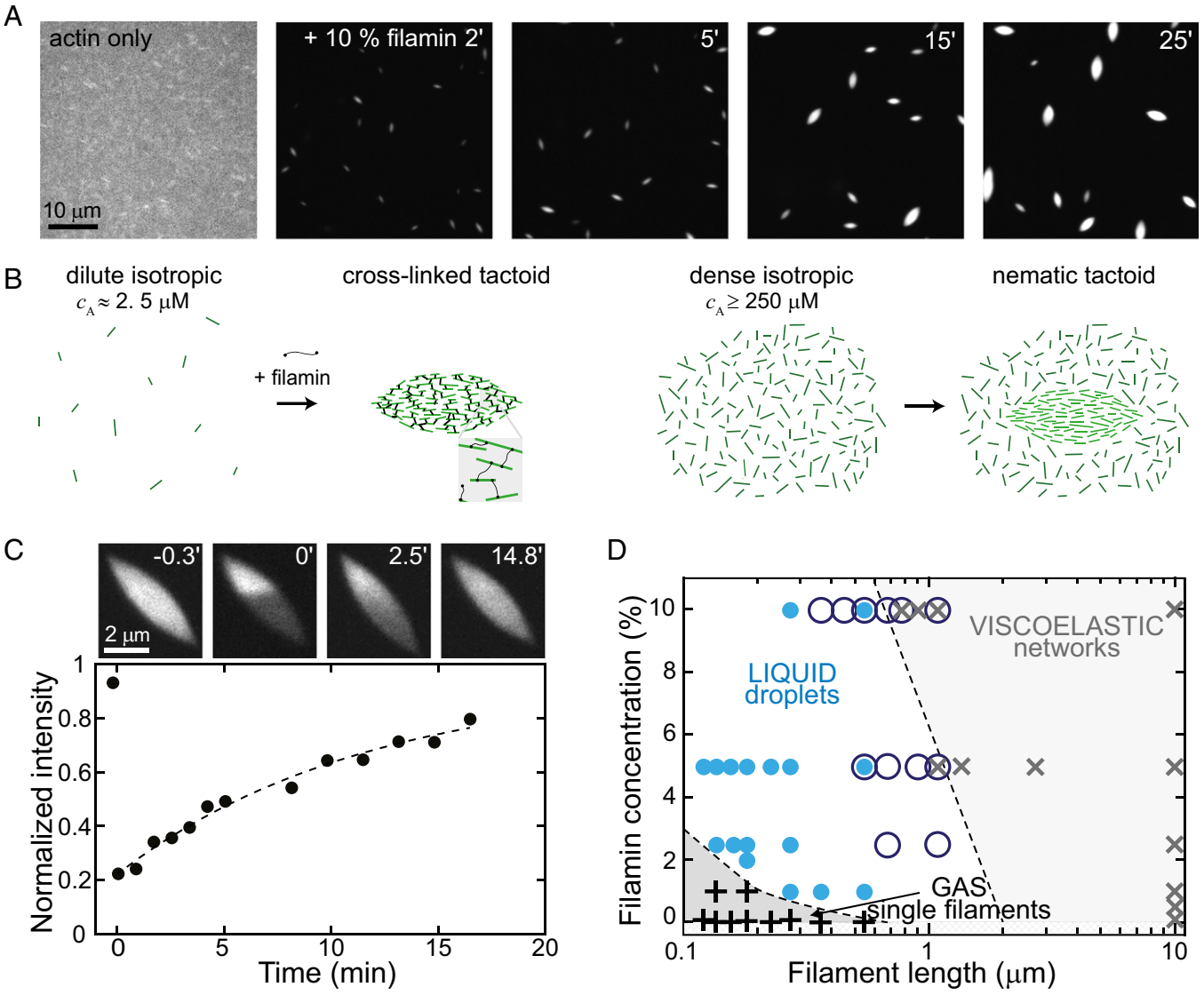

Fig. 1. Liquid droplets of cross-linked and short F-actin. (*A*) Fluorescence images of tetramethylrhodamine-labeled actin (TMR-actin) (1 mol % capping protein) before (actin only) and after addition of 10 mol % filamin (added at $t = 0$). (*B*) Tactoids are the shape of entropically formed liquid crystal droplets near the isotropic–nematic phase transition (*Right*). Here we observe tactoids induced by the addition of cross-linkers (*Left*). (*C*) Images of TMR-actin within a tactoid (1.5 mol % capping protein and 5 mol % filamin; *Upper*), with photobleaching occurring at $t = 0$ min. Average normalized TMR-actin intensity of the photobleached region over time (dashed line indicates exponential fit with $\tau_R = 880$ s). (*D*) Phase diagram of solid, liquid, and gas phases of cross-linked actin. Black plus symbols are data where dispersed filaments are observed, blue filled circles are samples exhibiting tactoid droplets, dark blue open circles are samples with fluid bundles (Fig. 4), and black crosses are samples where space spanning networks are observed.

concentrated suspensions of rods where entropic effects drive the nucleation of orientationally ordered droplets within a dense isotropic background (Fig. 1*B*, *Right*) (21, 22). For actin filaments of the length in our experiments, these phases occur at concentrations of ∼250 μM (23) (*SI Text*). Here we find that filamin induces the formation of tactoids at 100-fold lower actin concentration. In further contrast to traditional liquid crystal tactoids, cross-linked tactoids are surrounded by an undetectably low concentration of F-actin (Fig. 1*B*, *Left*).

To probe whether cross-linked actin tactoids are fluid, we investigate the actin filament mobility via fluorescence recovery after photobleaching (Fig. 1*C*, images, and Movie S2). After photobleaching a region of the tactoid, the F-actin fluorescence intensity recovers in the bleached region, suggesting that filaments rearrange within the tactoid (Fig. 1*C* and Fig. S1). We quantify the recovery by plotting the ratio of the fluorescence intensity on the bleached side to the unbleached side as a function of time. The increasing intensity ratio with time is fit to a rising exponential, yielding a recovery time of $\tau_R \sim 900$ s. From this, we estimate a diffusion coefficient of $D \sim 0.3 \times 10^{-2}$ μm^2/s and a viscosity, $\eta \sim 3$ Pa·s (*SI Text*), comparable to viscosities reported in other protein and colloid systems (24).

We observe tactoids over a range of actin filament lengths (0.1–1 μm) and filamin concentrations (1–10 mol %) (Fig. 1*D*). At longer filament lengths, we observe the formation of space-spanning actin networks, which have a viscoelasticity that has been well studied (25). At extremely low filament lengths or cross-link concentrations, tactoids do not form, and actin filaments freely diffuse in solution, analogous to a gas phase.

Tactoid Shape Can Be Modulated by Filament Cross-Linking. Thus far, we have only observed tactoid formation with filamin. Cross-links are typically thought of as interacting with the filaments in an anisotropic fashion, by promoting actin filament alignment.

However, filamin is a long (~150 nm) and flexible actin cross-linker, with transient binding kinetics (19). This may allow for a less orientationally constrained, long-range attractive interaction between filaments. Thus, cross-links may serve as a source of isotropic or anisotropic cohesion between filaments. To explore this, we form tactoids with variable filamin concentration from 2.5 to 15 mol % (Fig. 2*A*, images and open circles). We describe the resulting tactoid shape by the aspect ratio, L/r, where L and r are the major and minor axes lengths, respectively. At low filamin concentration, tactoids are elongated ($L/r \sim 3$ for 2.5 mol % filamin). Strikingly, we find that as the concentration of filamin cross-links increases, the tactoid aspect ratio decreases ($L/r \sim 2$ for 15 mol % filamin).

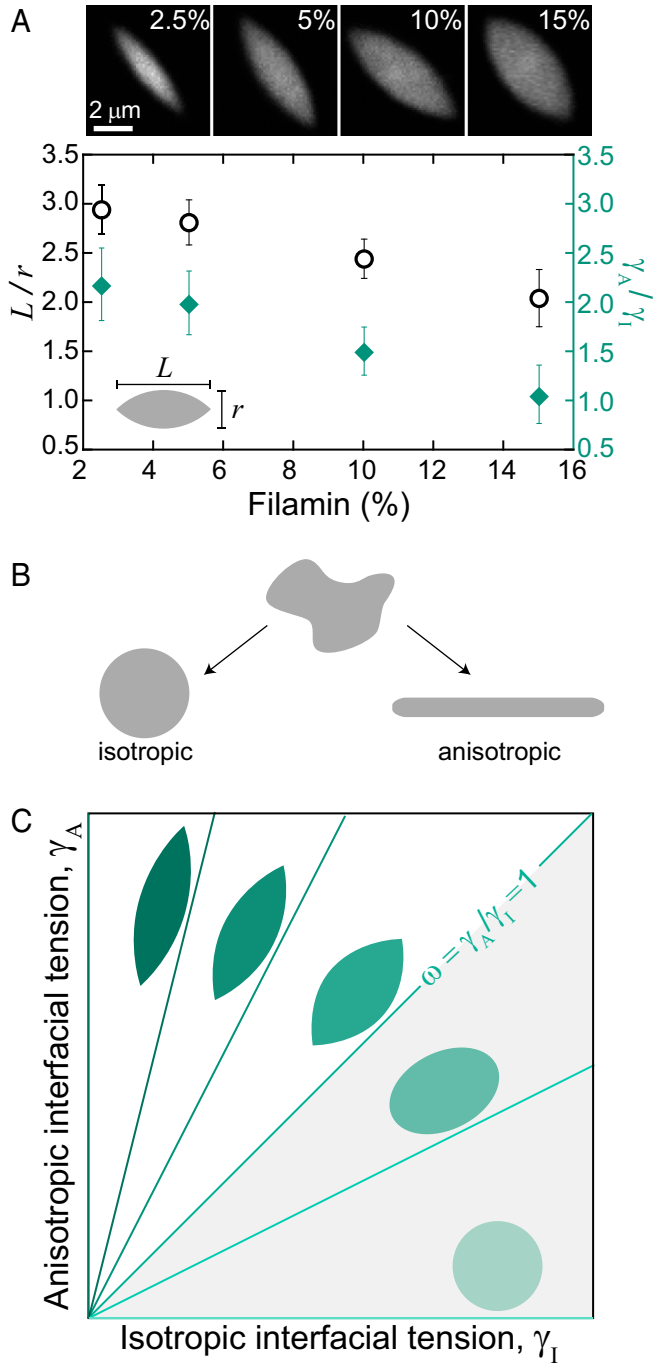

Fig. 2. Cross-linking regulates tactoid interfacial tension. (*A*) Tactoid (1.5 mol % capping protein) images, visualized with TMR-actin for filamin concentration from 2.5 to 15 mol %. Aspect ratio (black open circles) and ratio of anisotropic to isotropic interfacial tension, γ_A/γ_I (green diamonds), as a function of filamin concentration. (*B*) An arbitrary shaped liquid droplet with purely isotropic interfacial tension relaxes to an equilibrium shape of a sphere, whereas a droplet with purely anisotropic interfacial tension relaxes to an elongated, cylindrical equilibrium shape. (*C*) Model predictions of liquid droplet shape for varying isotropic and anisotropic interfacial tension ratios.

To understand tactoid shape, we model the tactoid as a fluid droplet using a continuum theory (*SI Text*). An ordinary liquid droplet has purely isotropic interfacial tension, and the optimal equilibrium shape is a sphere (Fig. 2*B*). In contrast, a liquid crystal droplet is made of anisotropic particles, which gives rise to an anisotropic interfacial tension (21). A collection of rods with purely anisotropic interactions would have a preferred equilibrium shape of a cylinder (Fig. 2*B*), with a tendency of rod-like particles to align with the interface. Thus, we model a tactoid as a droplet with both isotropic, γ_I, and anisotropic, γ_A, interfacial tension components (20, 21) (*SI Text* and Fig. S2). The optimal shape of the droplet is determined by minimizing the interfacial energy, controlled by a single dimensionless parameter, $\omega = \gamma_A/\gamma_I$. The balance of anisotropic and isotropic interfacial tensions yields elongated shapes for $\omega > 0$, which become increasingly elongated as ω grows and sharp features emerge for $\omega > 1$ (Fig. 2*C*).

We calculate ω from the experimentally observed aspect ratios using the theoretical relation $L/r = 2\omega^{1/2}$ for $\omega \geq 1$ (20) (*SI Text*). We observe that ω is inversely proportional to filamin concentration (Fig. 2*A*, diamonds). Thus, filamin alters ω such that the relative contribution of isotropic interfacial tension increases with respect to the anisotropic interfacial tension. This indicates that filamin serves primarily as cohesion between F-actin, rather than to enforce F-actin alignment within droplets.

Cross-Link Concentration Modulates Tactoid Shape Dynamics. Over 100 min, the average tactoid length increases as a power law, $L \sim t^{\alpha}$, where $\alpha = 0.47 \pm 0.01$ (Fig. 3*A*, dashed, and Movie S3). Notably, as the average size increases, the tactoid aspect ratio remains constant (Fig. 3*A*, open squares). This is consistent with theory and experiments on tactoids with homogeneous nematic alignment (26, 27) (*SI Text*).

Tactoid growth likely occurs via coarsening mechanisms associated with conventional liquid droplets, including Ostwald ripening and droplet coalescence (28). At the earliest observed stages of tactoid formation, there is a negligible concentration of F-actin in the bulk. This suggests that tactoid growth via single filament accretion, or Ostwald ripening, is unlikely. Instead, we observe individual coalescence events where two initially separate tactoids merge into a single elongated droplet that relaxes, within minutes, into a larger tactoid (Fig. 3*B*, images, and Movie S4). Moreover, the scaling exponent we measure in growth dynamics is consistent with that expected for coarsening of isotropic liquid droplets via interfacial tension-driven coalescence ($\alpha = 0.5$) (28).

As a further test that liquid properties dominate tactoid growth via coalescence, we probe the droplet deformation dynamics. We measure the tactoid length, L, along the major axis, over time as two initially separate tactoids coalesce (Fig. 3*B*). After initial coalescence ($L = L_i$), the length rapidly decreases as the merged droplet shape relaxes toward a steady-state tactoid shape with $L = L_f$. The length shortening is consistent with an exponential decay from which we extract a single characteristic relaxation time, τ, using $L(t) = L_f + (L_i - L_f)\exp(-t/\tau)$, where τ is a characteristic relaxation time (Fig. 3*B*, line). Data from multiple coalescence events collapse onto a single master curve upon rescaling the length by the deformation length, $L_i - L_f$, and time by τ (Fig. 3*C*).

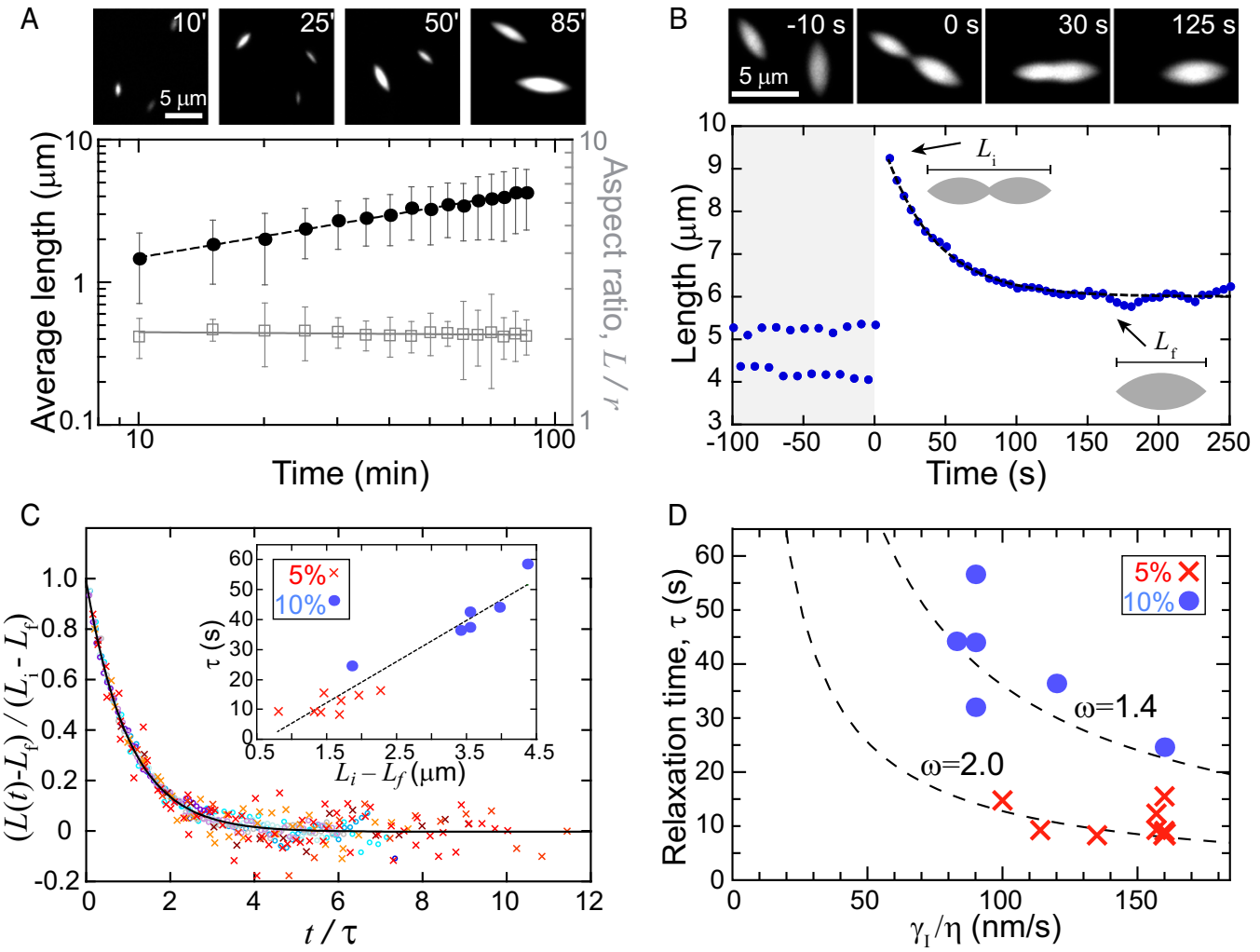

Fig. 3. Cross-link density regulates interfacial tension and viscosity. (*A*) Fluorescence images of tactoid growth (1.5 mol % capping protein and 5 mol % filamin), visualized by TMR-actin. Average tactoid length (black closed circles) and aspect ratio (open squares) are shown as a function of time after filamin addition, and dashed line indicates a power law fit $L \sim t^{\alpha}$, where $\alpha = 0.47 \pm 0.01$ for four datasets. Error bars represent ±1 SD. (*B*) Fluorescence images of tactoids (1 mol % capping protein and 10 mol % filamin) coalescence. Tactoid length, along the major axis, is shown as a function of time as two initially separate tactoids coalesce. Dashed line is an exponential fit. (*C*) Tactoid length, rescaled by the deformation length, as a function of time, rescaled by the characteristic relaxation time, for 14 coalescence events (1 mol % capping protein and 5 and 10 mol % filamin) collapses into a master curve. The solid line represents an exponential decay. (*Inset*) Linear scaling between relaxation time and deformation length from exponential fits of length relaxation. (*D*) The interfacial tension to viscosity ratio obtained from continuum model fits to the experimental data falls on the theoretically predicted curve for anisotropic droplets.

Using our continuum model for anisotropic fluids (*SI Text*), we can determine the tactoid shape dynamics during coalescence as function of γ_I, γ_A, and η and extract the characteristic shape relaxation timescale τ (*SI Text*). From the model, we calculate τ as a function of η/γ_I for varying values of $\omega = \gamma_A/\gamma_I$ (Fig. 3*D*, dashed lines). We find that τ obtained from experimental data for 5 and 10 mol % filamin is consistent with those predicted for $\omega = 2$ and 1.4 (values corresponding to those in Fig. 2*A*), respectively (Fig. 3*D*, symbols). Thus, the shape dynamics during droplet coalescence events can be quantitatively described with a continuum fluid model containing both isotropic and anisotropic interfacial tensions. From the η/γ_I obtained in the fit (Table S1), and the viscosity estimated from photobleaching, we estimate $\gamma_I \sim 300$ nN/m. This interfacial tension is ~10 times less than reported for other protein-based liquid droplets (24, 29) but consistent with theoretical predictions for larger particles such as actin filaments (21). Consistent with coalescence in isotropic droplets, we observe a linear scaling when we plot the relaxation time, τ, as a function of the deformation length, $L_i - L_f$, from the exponential fits (Fig. 3*C*, *Inset*). The slope of the line is η/γ_{eff}, where γ_{eff} is an effective interfacial tension with contributions from both γ_I and γ_A (*SI Text*). The data from the two different filamin concentrations fall on the same line, suggesting that that cross-link density modifies viscosity and the effective interfacial tension proportionally. Together, the droplet shape and dynamics demonstrate that filamin cross-link concentration modulates both the interfacial tensions and the viscosity of F-actin droplets.

Interfacial Tension Drives Pearling and Contraction of Bundles. Actin bundles formed with passive cross-linkers are typically thought to be kinetically trapped structures with few structural rearrangements at long times (12). However, our findings suggest that when the actin filaments are sufficiently short, we may be able to observe bundles displaying fluid-like behavior. We explore this in our system by constructing bundles near the liquid–solid boundary (Fig. 1*D*). We increased the actin filament length such that the initial assembly conditions create long (>50 μm), thin (radius

~200 nm) bundles of cross-linked F-actin within ~1 min (Fig. 4 *A* and *B*). After rapid assembly, these bundles continue to change shape over ~10 min timescales. Some bundles develop pearling instabilities along their length that evolve into periodically spaced bulges, which grow circumferentially in time (Fig. 4*A* and Movie S5). Such behavior is characteristic of a Rayleigh–Plateau instability observed in fluid columns, where interfacial tension drives the growth of periodic bulges that arise from fluctuations (*SI Text* and Fig. S3). In contrast to simple fluids, where capillary instabilities result in droplet breakup (30), we observe instabilities that evolve into chains of tactoids bridged by thin bundles. This is reminiscent of polymer fluids, where droplet breakup is arrested by polymer entanglements in the thinning bridges (31) (*SI Text*). The characteristic length scale of pearling is longer than that expected from a simple fluid, consistent with our theoretical model based on anisotropic interfacial tension (*SI Text*).

We also observe bundles that contract (Fig. 4*B* and Movies S6 and S7). The bundle length, $L(t)$ shortens exponentially in time, reducing in length by 20–60% over ~10 min (Fig. 4*C*) toward a tactoid shape. This length contraction is captured by our dynamic continuum model of a droplet relaxing to its equilibrium shape (*SI Text* and Fig. 4*C*). Upon rescaling $L(t)$ by deformation length, $L_i - L_f$, and time by the relaxation time, τ, we find that bundles across a range of cross-linking concentrations collapse onto a single exponential decay (Fig. 4*D*). This suggests that contracting bundles are also liquid columns that relax to their equilibrium shapes with a characteristic timescale. We find that the extent of cross-linking provides a tunable parameter to modulate bundle contractile strain and strain rates (Fig. 4*E*). Thus, if cross-linked F-actin bundles are fluidized, interfacial tension is sufficient to drive their contractility.

Discussion

The experimental characterization of cytoskeletal liquid crystal phases is a nascent field (15, 23, 32, 33). Here we describe a liquid crystal droplet, induced by the addition of cross-links and phase separated from a dilute suspension of anisotropic particles. We find that the physiological cross-linker filamin cross-links short F-actin into liquid crystalline droplets at concentrations 100-fold less than the critical concentration expected for entropic ordering. In this unusual, cross-linked liquid crystal, cross-linkers provide attractive interactions, allowing for the modulation of liquid properties such as interfacial tension and viscosity. The liquid phase is likely supported by filamin's biophysical properties: filamin is a long (~150 nm) and flexible actin cross-linker, with transient binding kinetics (19). We hypothesize that these cross-link properties are crucial to allowing filament orientational and translational mobility to support a liquid

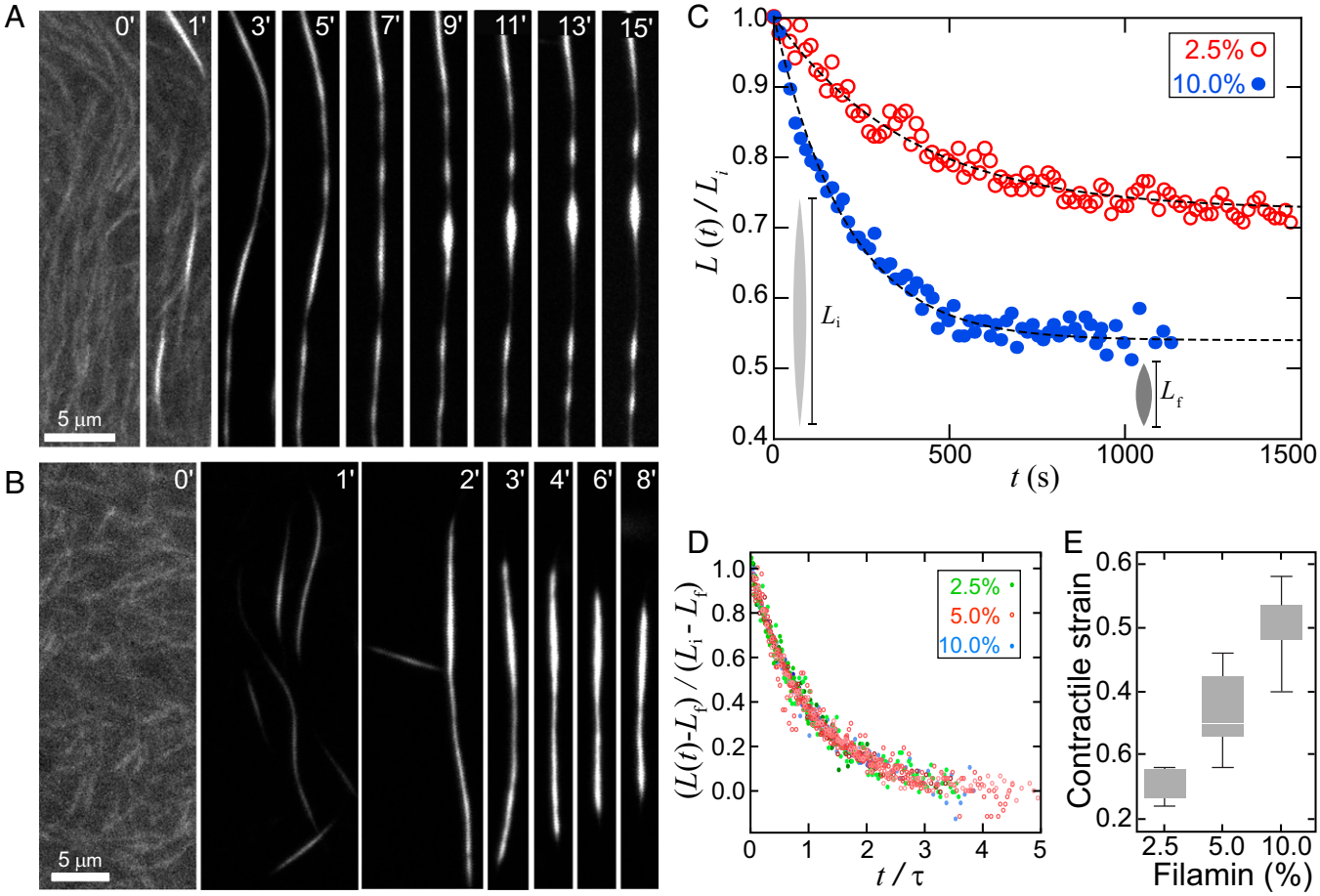

Fig. 4. Interfacial tension drives instabilities and contraction in fluid F-actin bundles, visualized with TMR-actin. (*A*) Fluorescence images of an F-actin bundle (0.5 mol % capping protein and 10 mol % filamin) that exhibits instabilities that grow over time. (*B*) Fluorescence images of an F-actin bundle (0.25 mol % capping protein and 10 mol % filamin) that shortens over time. (*C*) Bundle length (0.25 mol % capping protein and 2.5 mol %, and 10 mol % filamin) as a function of time. (*D*) Bundle length, rescaled by the deformation length, as a function of time, rescaled by the characteristic relaxation time collapses on to a single master curve (0.25 mol % capping protein and 2.5, 5, and 10 mol % filamin). (*E*) Contractile strain increases with cross-linker concentration. Contrast is separately adjusted for prebundled actin images (*A*, 0′, 1′; *B*, 0′).

phase. Understanding the molecular mechanisms to control macromolecular liquid phases is an exciting avenue of future research.

Evidence of liquid phases of cross-linked biopolymers in vitro potentially has significant implications for cytoskeletal architecture and mechanics. Liquid crystal physics has been invoked to describe the meiotic spindle shape (15) and actomyosin flows (5). Cross-linked biopolymer tactoids provide a minimal model system to explore biopolymer liquid crystals. Our data provide evidence for a liquid crystal description of spindle shape (15, 34, 35), physical properties (15), and scaling with system size (36). These results suggest that liquid crystal theory has the potential to describe diverse biopolymer assemblies beyond the actin and microtubule cytoskeleton, including amyloid fibrils, intermediate filaments, and bacterial homologs of actin and microtubules.

Transitions between solid and liquid phases change the underlying physical properties of materials. Regulatory proteins in vivo provide dynamic control of biopolymer filament length and cross-link affinity, which could potentially drive the system between a gel and liquid phase to alter bundle mechanics and shape. Most notably, we find that bundles of fluid cross-linked filaments relax their shape by contracting, without requiring molecular motor activity. These results demonstrate that interfacial tension is sufficient to drive shortening and shape instabilities of bundles, suggesting a mechanism for previously reported motor-independent contraction in cells (37). Future research will elucidate the extent to which liquid phases of biopolymer filaments organize the interior of living cells and how such biological structures can inform novel soft materials design.

ACKNOWLEDGMENTS. We acknowledge T. Thoresen and S. Stam for purified filamin and C. Suarez and D. R. Kovar for capping protein. This research was supported by the University of Chicago Materials Research Science and Engineering Center (National Science Foundation Division of Materials Research Grant 1420709). M.L.G. acknowledges support from National Science Foundation Molecular Cellular Biosciences Grant 1344203. S.B. acknowledges support from the Institute for the Physics of Living Systems at University College London. S.V. acknowledges support from the University of Chicago.

1. Alberts B, et al. (2015) *Molecular Biology of the Cell* (Garland Science, New York), 6th Ed, pp 1–1342.
2. Parsons JT, Horwitz AR, Schwartz MA (2010) Cell adhesion: Integrating cytoskeletal dynamics and cellular tension. *Nat Rev Mol Cell Biol* 11(9):633–643.
3. Lecuit T, Lenne PF, Munro E (2011) Force generation, transmission, and integration during cell and tissue morphogenesis. *Annu Rev Cell Dev Biol* 27(27):157–184.
4. Blanchoin L, Boujemaa-Paterski R, Sykes C, Plastino J (2014) Actin dynamics, architecture, and mechanics in cell motility. *Physiol Rev* 94(1):235–263.
5. Prost J, Julicher F, Joanny JF (2015) Active gel physics. *Nat Phys* 11(2):111–117.
6. Guillot C, Lecuit T (2013) Mechanics of epithelial tissue homeostasis and morphogenesis. *Science* 340(6137):1185–1189.
7. Fletcher DA, Mullins RD (2010) Cell mechanics and the cytoskeleton. *Nature* 463(7280):485–492.
8. Stricker J, Falzone T, Gardel ML (2010) Mechanics of the F-actin cytoskeleton. *J Biomech* 43(1):9–14.
9. Gardel ML, Kasza KE, Brangwynne CP, Liu JY, Weitz DA (2008) Mechanical response of cytoskeletal networks. *Biophysical Tools for Biologists: Vol. 2, In Vivo Techniques*, Methods in Cell Biology (Academic, San Diego), Vol 89, pp 487–519.
10. Broedersz CP, MacKintosh FC (2014) Modeling semiflexible polymer networks. *Rev Mod Phys* 86(3):995–1036.
11. Falzone TT, Lenz M, Kovar DR, Gardel ML (2012) Assembly kinetics determine the architecture of α-actinin crosslinked F-actin networks. *Nat Commun* 3:861.
12. Lieleg O, Kayser J, Brambilla G, Cipelletti L, Bausch AR (2011) Slow dynamics and internal stress relaxation in bundled cytoskeletal networks. *Nat Mater* 10(3):236–242.
13. Murrell M, Oakes PW, Lenz M, Gardel ML (2015) Forcing cells into shape: The mechanics of actomyosin contractility. *Nat Rev Mol Cell Biol* 16(8):486–498.
14. Viamontes J, Tang JX (2003) Continuous isotropic-nematic liquid crystalline transition of F-actin solutions. *Phys Rev E Stat Nonlin Soft Matter Phys* 67(4 Pt 1):040701.
15. Brugués J, Needleman D (2014) Physical basis of spindle self-organization. *Proc Natl Acad Sci USA* 111(52):18496–18500.
16. Hyman AA, Weber CA, Juelicher F (2014) Liquid-liquid phase separation in biology. *Annual Review of Cell and Developmental Biology*, eds Schekman R, Lehmann R (Annual Reviews, Palo Alto, CA), Vol 30, pp 39–58.
17. Weeds A, Maciver S (1993) F-actin capping proteins. *Curr Opin Cell Biol* 5(1):63–69.
18. Schmidt CF, Barmann M, Isenberg G, Sackmann E (1989) Chain dynamics, mesh size, and diffusive transport in networks of polymerized actin: A quasielastic light-scattering and microfluorescence study. *Macromolecules* 22(9):3638–3649.
19. Nakamura F, Stossel TP, Hartwig JH (2011) The filamins: Organizers of cell structure and function. *Cell Adhes Migr* 5(2):160–169.
20. Prinsen P, van der Schoot P (2003) Shape and director-field transformation of tactoids. *Phys Rev E Stat Nonlin Soft Matter Phys* 68(2 Pt 1):021701.
21. de Gennes PG, Prost J (1993) *The Physics of Liquid Crystals* (Clarendon Press, Oxford).
22. Onsager L (1949) The effects of shape on the interaction of colloidal particles. *Ann N Y Acad Sci* 51(4):627–659.
23. Oakes PW, Viamontes J, Tang JX (2007) Growth of tactoidal droplets during the first-order isotropic to nematic phase transition of F-actin. *Phys Rev E Stat Nonlin Soft Matter Phys* 75(6 Pt 1):061902.
24. Brangwynne CP, et al. (2009) Germline P granules are liquid droplets that localize by controlled dissolution/condensation. *Science* 324(5935):1729–1732.
25. Lieleg O, Claessens M, Bausch AR (2010) Structure and dynamics of cross-linked actin networks. *Soft Matter* 6(2):218–225.
26. Prinsen P, van der Schoot P (2004) Continuous director-field transformation of nematic tactoids. *Eur Phys J E Soft Matter* 13(1):35–41.
27. Jamali V, et al. (2015) Experimental realization of crossover in shape and director field of nematic tactoids. *Phys Rev E Stat Nonlin Soft Matter Phys* 91(4):042507.
28. Bray AJ (2002) Theory of phase-ordering kinetics. *Adv Phys* 51(2):481–587.
29. Elbaum-Garfinkle S, et al. (2015) The disordered P granule protein LAF-1 drives phase separation into droplets with tunable viscosity and dynamics. *Proc Natl Acad Sci USA* 112(23):7189–7194.
30. Eggers J, Villermaux E (2008) Physics of liquid jets. *Rep Prog Phys* 71(3):036601.
31. Eggers J (2014) Instability of a polymeric thread. *Phys Fluids* 26(3):033106.
32. Sanchez T, Chen DTN, DeCamp SJ, Heymann M, Dogic Z (2012) Spontaneous motion in hierarchically assembled active matter. *Nature* 491(7424):431–434.
33. Safinya CR, Deek J, Beck R, Jones JB, Li YL (2015) Assembly of biological nanostructures: Isotropic and liquid crystalline phases of neurofilament hydrogels. *Annual Review of Condensed Matter Physics*, ed Langer JS (Annual Reviews, Palo Alto, CA), Vol 6, pp 113–136.
34. Young S, Besson S, Welburn JPI (2014) Length-dependent anisotropic scaling of spindle shape. *Biol Open* 3(12):1217–1223.
35. Helmke KJ, Heald R (2014) TPX2 levels modulate meiotic spindle size and architecture in Xenopus egg extracts. *J Cell Biol* 206(3):385–393.
36. Good MC, Vahey MD, Skandarajah A, Fletcher DA, Heald R (2013) Cytoplasmic volume modulates spindle size during embryogenesis. *Science* 342(6160):856–860.
37. Neujahr R, Heizer C, Gerisch G (1997) Myosin II-independent processes in mitotic cells of Dictyostelium discoideum: Redistribution of the nuclei, re-arrangement of the actin system and formation of the cleavage furrow. *J Cell Sci* 110(Pt 2):123–137.
38. Weirich KL, Israelachvili JN, Fygenson DK (2010) Bilayer edges catalyze supported lipid bilayer formation. *Biophys J* 98(1):85–92.
39. Spudich JA, Watt S (1971) The regulation of rabbit skeletal muscle contraction. I. Biochemical studies of the interaction of the tropomyosin-troponin complex with actin and the proteolytic fragments of myosin. *J Biol Chem* 246(15):4866–4871.
40. Palmgren S, Ojala PJ, Wear MA, Cooper JA, Lappalainen P (2001) Interactions with PIP2, ADP-actin monomers, and capping protein regulate the activity and localization of yeast twinfilin. *J Cell Biol* 155(2):251–260.
41. Craig SW, Lancashire CL, Cooper JA (1982) Preparation of smooth muscle alpha-actinin. *Methods Enzymol* 85(Pt B):316–321.
42. Rasband WS (1997–2012) ImageJ (US National Institutes of Health, Bethesda, MD).
43. Berg HC (1983) *Random Walks in Biology* (Princeton University Press, Princeton).
44. Rapini A, Papoular MJ (1969) Distortion d'une lamelle nématique sous champ magnétique conditions d'ancrage aux parois. *J Phys Colloq* 30:C4–C54.
45. Kaznacheev AV, Bogdanov MM, Taraskin SA (2002) The nature of prolate shape of tactoids in lyotropic inorganic liquid crystals. *J Exp Theor Phys* 95(1):57–63.
46. Virga EG (1994) *Variational Theories for Liquid Crystals* (Chapman and Hall, London).
47. Papageorgiou DT (1995) On the breakup of viscous-liquid threads. *Phys Fluids* 7(7):1529–1544.
48. Cheong AG, Rey AD, Mather PT (2001) Capillary instabilities in thin nematic liquid crystalline fibers. *Phys Rev E Stat Nonlin Soft Matter Phys* 64(4 Pt 1):041701.
49. Powers TR, Goldstein RE (1997) Pearling and pinching: Propagation of Rayleigh instabilities. *Phys Rev Lett* 78(13):2555–2558.